Electronic Supplementary Material (ESI) for Journal of Materials Chemistry B.

Supporting Information

The sodium hyaluronate microspheres fabricated by solution drying for transcatheter arterial embolization

Zihan Yi[a,b], Zhichao Sun[c],Yang Shen[a,b], Dandan Luo[a,b], Rui Zhang[a,b], Shitu Ma[a,b], Ruibo Zhao[a,b], Jabeen Farheen[a,b], Muhanmmed Zubair Iqbal[a,b] and Xiangdong Kong[a,b,*]

[a]Institute of Smart Biomedical Materials, School of Materials Science and Engineering, Zhejiang Sci-Tech University, Hangzhou, 310018, China
[b]Zhejiang-Mauritius Joint Research Center for Biomaterials and Tissue Engineering, Hangzhou, 310018, China
[c]The Department of Medical Imaging, The First Medical College of Zhejiang Chinese Medical University, Hangzhou 310053, China
[*]*E-mail: kongxd@zstu.edu.cn*

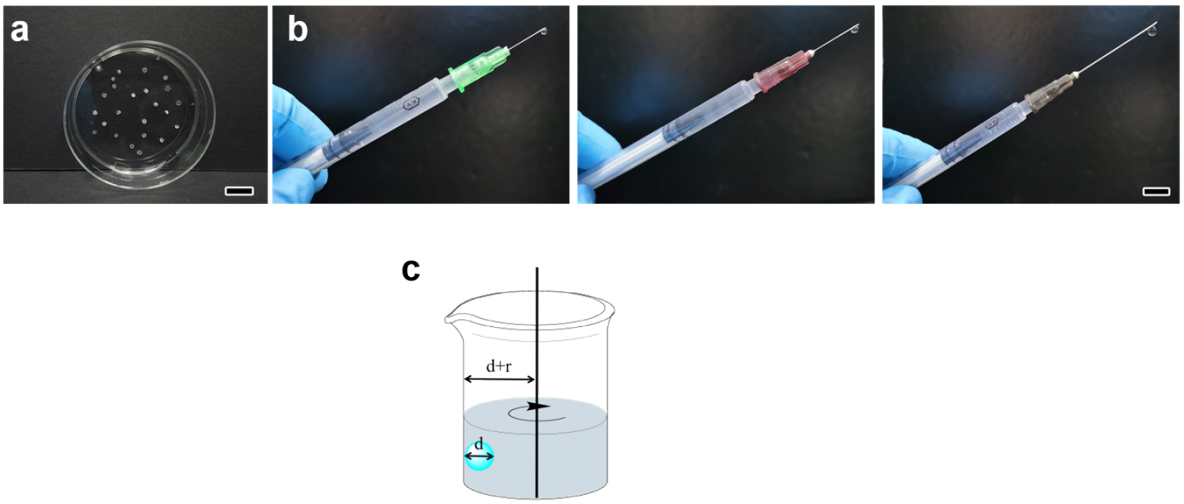

Fig. S1 (a) The images of obtained dry-droplets without dynamic stirring, scale bar, 2cm**.** (b)The images of gel dropets obtained with different needles, scale bar, 1cm. (c) The parameters illustration of a droplet during the process of dynamic stirring.

The gel droplets were drop into the isobutanol and stand for a while rather than a stirring. As shown in Fig.S1, the obtained dry-droplets adhere to the plate as the white precipitate instead of microspheres. It suggested the high-speed stirring is the key factor of the microspheres fabrication and the gel droplets are soft and weak to keep a sphere without dynamic condition. In addition, the origin droplets obtained with different needls was shown in Fig.S1b, it show an increase diameter of origin droplets which provide a initial conditions in the shape change of microspheres. The parameters illustration of a droplet (Fig. S1c) was added to help explain the formula:

$$\Delta P = pw^2\left[(r+d)^2 - r^2\right]/2.$$

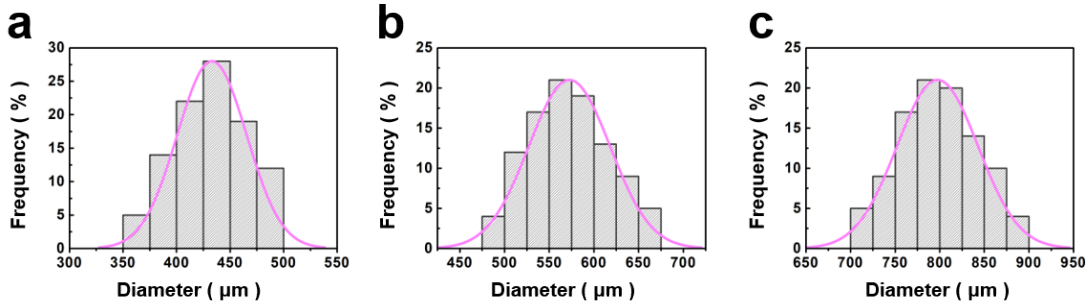

Fig. S2 Size distribution profile of SH microspheres prepared by needles with the size of 32G, 30G, and 28G after initial filter according to the commercial embolic microspheres.

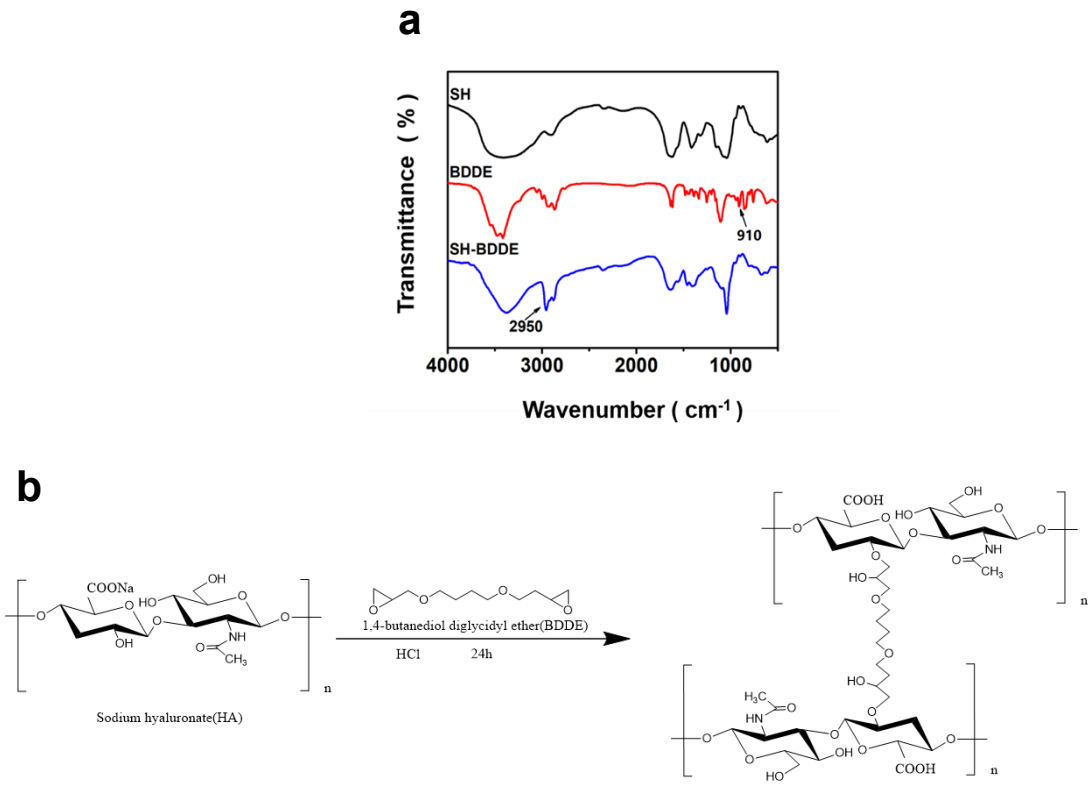

Fig. S4 (a) Respective FT-IR spectra of SH (powder), BDDE, SH-BDDE (SH microspheres). (b) The chemical reactions between BDDE and SH powder in HCl (aq).

The spectrum of SH powder possessed the characteristic absorption bands, particularly the stretching vibrations of O–H/N–H bond at 3382 cm^{-1}, C–H bond at 2904 cm^{-1}, C=O bond at 1624 cm^{-1}, amide-II at 1564 cm^{-1}, C–O bond of –COONa group at 1410 cm^{-1}, and C–O–C bond at 1039 cm^{-1}. In addition, the FTIR peaks of SH powder at 1321 cm^{-1} and 944 cm^{-1} correspond to the vibrations of C–H bending and C–O–H deformation, respectively. The spectrum of BDDE showed the characteristic peaks including the C–H stretching of the epoxy ring at 2925 cm^{-1}, the C–H stretching of $–CH_2$ bond at 2860 cm^{-1}, the C–C bond at 1254 cm^{-1}, the C–O–C stretching at 1106 cm^{-1}, and C–O stretching vibrations of the epoxy ring at 910 cm^{-1}.

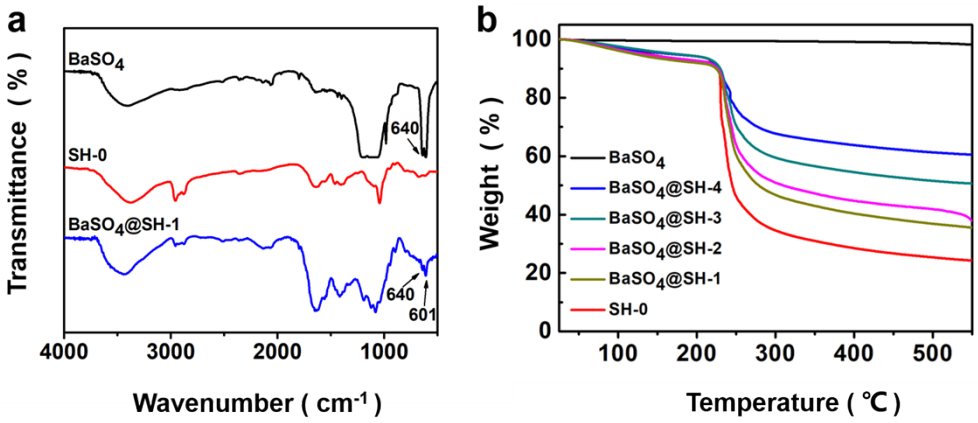

Fig. S5 Characterizations of $BaSO_4$@SH microspheres: (a) FTIR spectra of $BaSO_4$ NPs, SH microspheres, and $BaSO_4$@SH-1 microspheres; (b) TGA curves of $BaSO_4$ NPs, SH-0 microspheres, and $BaSO_4$@SH microspheres.

For the FTIR spectrum of $BaSO_4$, peaks at 1046–1200 and 979 cm^{-1} are assigned to the symmetrical vibrations of SO_4^{2-} and peaks at 601 and 640 cm^{-1} are attributed to the out-of-plane bending vibration of SO_4^{2-}.

As shown in Fig. S5b, there is bare weight loss for $BaSO_4$ during an apparent weight loss for both SH-0 microspheres and $BaSO_4$@SH microspheres. This suggested that the $BaSO_4$ has excellent thermal stability as compared to SH. There are two phases of weight loss seen in SH-0 microspheres and $BaSO_4$@SH microspheres at the same temperatures. For the first weight loss between 30 and 220 ℃, the physically adsorbed water was removed from microspheres due to the high-temperature environment, which occurred slowly. While for the second phase of weight loss (220 and 500 ℃), a rapid weight loss behavior is observed, which could be ascribed to the decomposition of the SH chains. After heating at 500 ℃, there was no apparent weight loss in the TGA curves

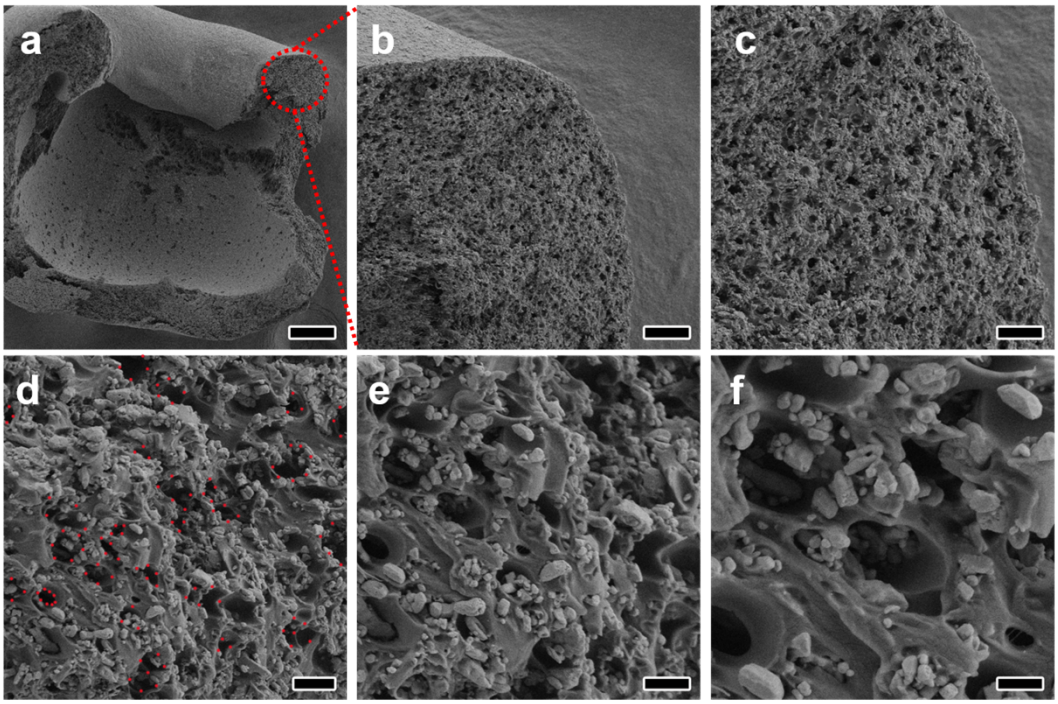

Fig. S6 (a-f) the SEM images of a single cut $BaSO_4$@SH microsphere with several amplifications, scale bar, 100 μm, 20 μm, 10μm, 3μm, 2μm, 1μm.

The above SEM images proved the exist of porous structure inside the $BaSO_4$@SH microsphere after adding the $BaSO_4$ NPs.

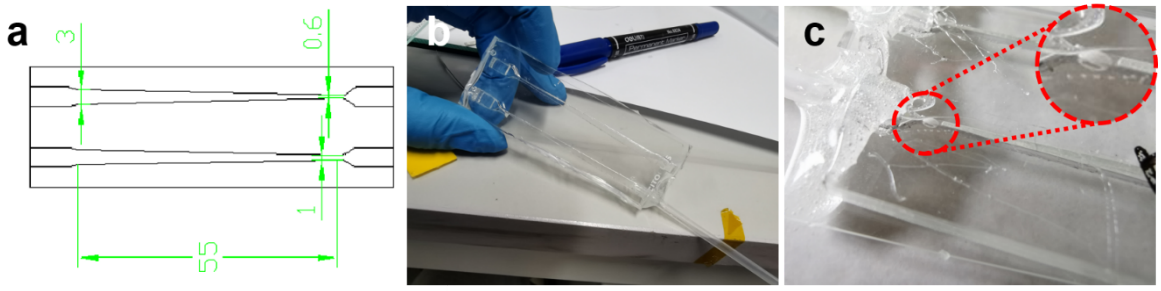

Fig. S7 (a) The design image of the PDMS chip, mm. (b) The PDMS chip connected with a catheter. (c) $BaSO_4$@SH-4 embolized in the PDMS chip after the compression test.

PDMS chip of a specific size was prepared and connected using a catheter. The system shown in Fig. S8 used the PDMS chip to conduct the compression test. As shown in Fig. S7c, a $BaSO_4$@SH-4 was delivered into the PDMS chip with excellent compressibility.

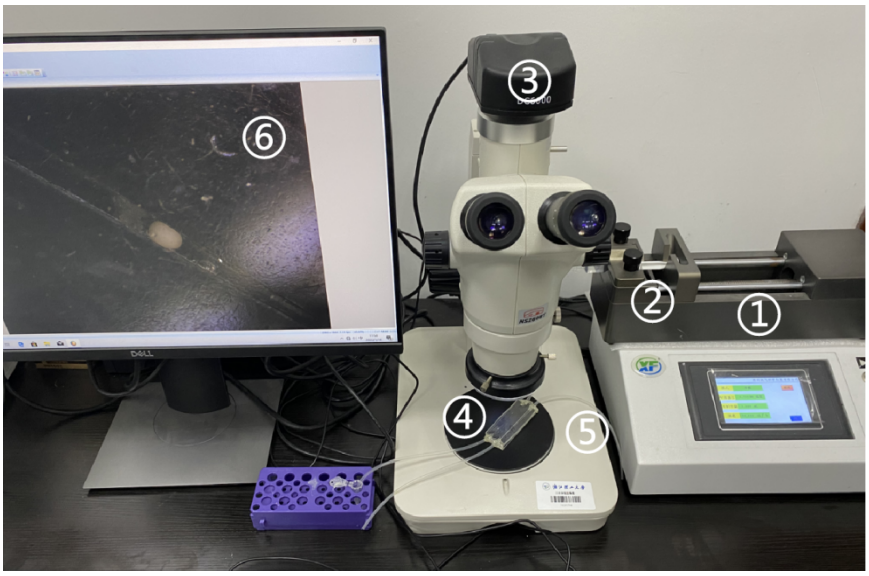

Figure. S8 A self-built system for compression test (1) Injection pump, (2) Syringe, (3) Stereoscope, (4) Connected PDMS chip, (5) Catheter, and (6) Recording screen.

The single microsphere with 20 mL PBS was added to the syringe and injected into the PDMS chip shown in Fig. S7 under pressure from the syringe pump, and their compressed images in PDMS chips were observed and captured via the stereoscope and computer.

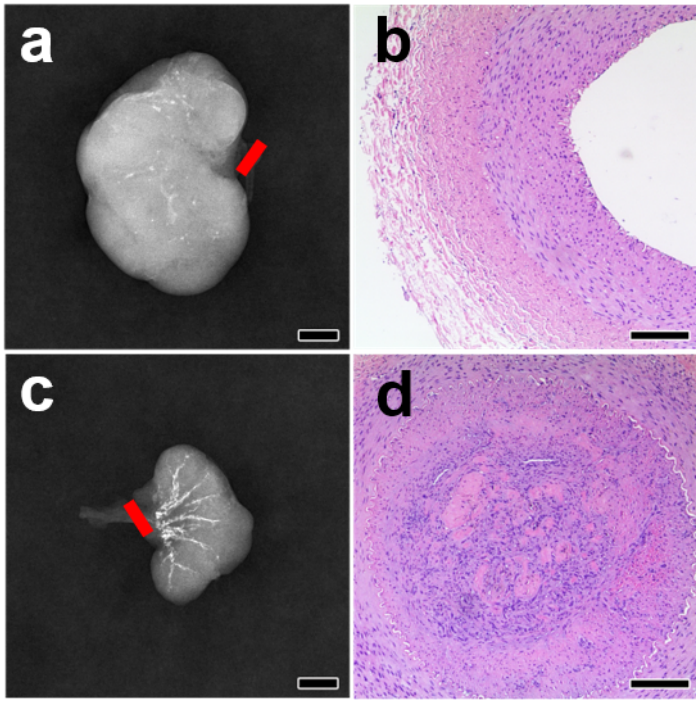

Fig. S9 Histopathological examination of dog kidneys tissue: (a) CT image of unembolized kidney collected at 4 weeks, scale bar, 2 cm. (b) H&E staining of the renal artery of (a), scale bar, 100 μm. (c) the enlarged view of (c), scale bar, 200 μm. (d) CT image of embolized kidney collected at 4 weeks, scale bar, 2 cm. (e) H&E staining of the renal artery of (d), scale bar, 100 μm. (f) the enlarged view of (c), scale bar, 200 μm.

Table. S1 Composition of the $BaSO_4$@SH microsphere.

Subgroup	HA (g)	BDDE (μL)	$BaSO_4$ (g)	HCl (mL)	Theoretical $BaSO_4$ contents (wt %)	Practical $BaSO_4$ contents (%)
SH-0	0.4	50	0.00	20	0.00	0.00
$BaSO_4$@SH-1	0.4	50	0.05	20	12.35	11.93
$BaSO_4$@SH-2	0.4	50	0.10	20	20.00	16.29
$BaSO_4$@SH-3	0.4	50	0.20	20	33.33	26.01
$BaSO_4$@SH-4	0.4	50	0.40	20	50.00	35.31

Table. S2 Young's modulus of $BaSO_4$@SH-4 and Embosphere® microspheres (n = 3)

Microspheres	$BaSO_4$@SH-4 (700-900 μm)	Embosphere®（700-900 μm）
Young's Modulus (kPa)	6.36 ± 0.9	28.6 ± 1.3